

# Revisiting Multi-Task Visual Representation Learning

Shangzhe Di<sup>1,2</sup> Zhonghua Zhai<sup>2</sup> Weidi Xie<sup>1</sup>

<sup>1</sup>SAI, Shanghai Jiao Tong University <sup>2</sup>ByteDance Seed

[github.com/Becomebright/MTV](https://github.com/Becomebright/MTV)

## Abstract

Current visual representation learning remains bifurcated: vision-language models (e.g., CLIP) excel at global semantic alignment but lack spatial precision, while self-supervised methods (e.g., MAE, DINO) capture intricate local structures yet struggle with high-level semantic context. We argue that these paradigms are fundamentally complementary and can be integrated into a principled multi-task framework, further enhanced by dense spatial supervision. We introduce **MTV**, a multi-task visual pretraining framework that jointly optimizes a shared backbone across vision-language contrastive, self-supervised, and dense spatial objectives. To mitigate the need for manual annotations, we leverage high-capacity “expert” models—such as Depth Anything V2 and OWLv2—to synthesize dense, structured pseudo-labels at scale. Beyond the framework, we provide a systematic investigation into the mechanics of multi-task visual learning, analyzing: (i) the marginal gain of each objective, (ii) task synergies versus interference, and (iii) scaling behavior across varying data and model scales. Our results demonstrate that MTV achieves “best-of-both-worlds” performance, significantly enhancing fine-grained spatial reasoning without compromising global semantic understanding. Our findings suggest that multi-task learning, fueled by high-quality pseudo-supervision, is a scalable path toward more general visual encoders.

## 1. Introduction

Recent advances in foundation models have reshaped visual representation learning by scaling pretraining on web-scale data. Currently, two paradigms prevail: *Vision-language (VL) contrastive learning* [19, 33, 49] aligns global image and text embeddings via instance-level discrimination, enabling open-vocabulary recognition and zero-shot transfer. *Self-supervised learning (SSL)*, such as masked image modeling [16, 51], contrastive instance discrimination [7, 15], and student-teacher matching [5, 32], enforces invariance and regularities without manual labels. Despite their suc-

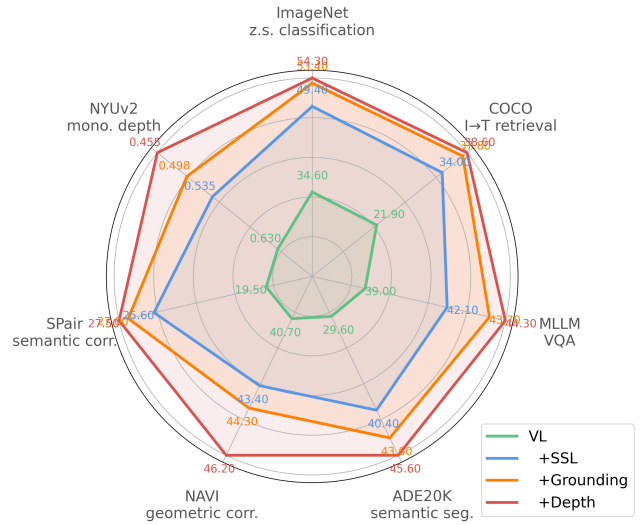


Figure 1. **Multi-task supervision effects** on a ViT-L model with 10M training samples. We integrate VL, SSL, and pseudo-labeled grounding and depth estimation into a unified training framework. This leads to strong and consistent performance gains across diverse vision and vision-language tasks.

cess, these paradigms remain bifurcated, primarily focusing on either global semantics or local regularities while leaving fine-grained spatial and geometric reasoning as under-constrained emergent properties. Given the inherent diversity of visual tasks—ranging from low-level geometry to high-level reasoning—learning truly universal visual representations that bridge these multifaceted requirements remains an open and fundamental challenge [10, 26, 38, 39].

In contrast, large language models (LLMs) scale effectively by absorbing multifaceted supervision—such as summarization, translation, and question answering—within a unified training interface [1, 4, 21]. Admittedly, unlike the discrete and sequential nature of language, visual tasks are inherently heterogeneous. While this diversity makes a single, universal objective more elusive in vision, we argue that visual pretraining can still embrace the LLM philosophy by simultaneously optimizing across a diverse suite of tasks to capture the full spectrum of information. Inspired by this

versatility, we ask: *Can visual pretraining be scaled by integrating semantic, spatial, and geometric supervision within a single, principled framework?*

To bridge this gap, we introduce **MTV**, a multi-task visual pretraining framework that jointly optimizes a shared backbone across vision-language contrastive, self-supervised, and dense spatial objectives. To overcome the scarcity of human-labeled data, we leverage high-capacity “expert” models—such as Depth Anything V2 [45] for monocular depth estimation and OWLv2 [29] for open-vocabulary grounding—to synthesize dense, structured pseudo-labels at scale. By integrating these expert-guided targets, we enrich traditional objectives with explicit geometric and spatial priors.

In this work, we go beyond simple multi-tasking to provide a systematic investigation into the mechanics of multi-task visual learning. By unifying these paradigms into a single encoder, we create a controlled setting to study how heterogeneous signals cooperate. Specifically, we examine: (i) the marginal gain of each objective, (ii) the dynamics of task synergies versus interference, and (iii) scaling behavior across varying data and model scales. Empirically, MTV achieves “best-of-both-worlds” performance, yielding representations that are both more general and more data-efficient than any single objective alone. For instance, our ViT-Base model trained on 100M samples achieves 69.4% ImageNet zero-shot accuracy—outperforming CLIP-Base [33] trained on 400M samples—while delivering substantial gains across retrieval, depth estimation, segmentation, and correspondence benchmarks. These results demonstrate that multi-task visual pretraining with high-quality pseudo-supervision enables the encoder to capture fine-grained, spatially grounded cues absent in pure vision-language models.

Taken together, these findings suggest a clear design principle: expanding conventional visual pretraining with complementary tasks—even when supervised by imperfect pseudo labels—shifts learning toward a unified, multi-granularity representation space. This unification, analogous in spirit to the convergence of diverse language tasks for LLM, offers a scalable and data-efficient pathway for building versatile visual encoders capable of anchoring a wide range of perception and multimodal reasoning tasks.

## 2. Related Work

**Self-supervised Learning (SSL).** Self-supervised visual pretraining aims to learn transferable representations without manual annotations. Contrastive and distillation-based methods, such as DINO [5], iBOT [51], and I-JEPA [2], encourage feature invariance across augmented views, whereas reconstruction-based approaches, like MAE [16], rely on masked image modeling. Recent large-scale efforts such as DINoV2 [32] demonstrate that scaling data and

model size leads to robust features for recognition, segmentation, and correspondence tasks. However, these methods remain limited to unimodal visual signals and lack semantics from natural language or high-level reasoning [38].

**Vision-Language Contrastive Learning (VL).** Weakly-supervised vision-language pretraining has emerged as a dominant paradigm for learning semantic-aligned visual encoders. CLIP [33] and ALIGN [19] show that large-scale vision-language contrastive learning yields powerful zero-shot transfer. Subsequent works such as Florence [47] and SigLIP [49] further improve alignment quality and scalability through better data curation and sigmoid-based objectives. Despite their impressive semantic generalization, these models are optimized purely for global alignment and often underperform on spatially structured or geometric tasks such as depth and correspondence estimation [10].

**Self-Training (ST).** Self-training refers to using a supervised model to generate pseudo labels on unlabeled data, followed by training a student model on these pseudo-labeled samples [43]. This paradigm has been widely adopted to expand supervision beyond human-annotated datasets. For VL contrastive learning, several approaches [11, 23, 25, 46] leverage language or vision-language models to generate synthetic captions or rewrite noisy web captions to enhance CLIP-style training. However, textual descriptions alone cannot fully capture the rich visual content within images. Beyond VL pretraining, self-training has also demonstrated remarkable success in other visual domains. For instance, Depth Anything [44, 45] first trains a teacher model on high-quality synthetic depth data and then uses it to generate pseudo labels on real images for student training, leading to state-of-the-art monocular depth estimation. Similarly, OWLv2 [29] employs a supervised open-vocabulary detector to produce billion-scale pseudo labels for scaling. Overall, self-training has emerged as an effective strategy for scaling visual supervision by leveraging strong teacher models to generate reliable annotations at an unprecedented scale. We build upon this trend by extending self-training to multi-task settings that combine VL and SSL objectives, enabling more general and scalable visual representation learning.

**Multi-task Visual Representation Learning.** Multi-task learning is a training paradigm where a model is jointly optimized on multiple tasks, leveraging shared representations to capture common structures and improve generalization across them. Recent progress in SSL, VL, and ST has inspired efforts to combine these paradigms for building more general visual encoders. Methods such as SLIP [30], SILC [31], and TIPS [27] show that integrating VL and SSL objectives yields complementary supervision, improving both semantic alignment and spatial understanding. In the context of ST, MuST [14] pioneered the idea that com-

bining multiple self-training tasks can yield stronger representations than purely supervised or self-supervised learning. Building upon this direction, we employ stronger and open-vocabulary teacher models and integrate them with VL and SSL objectives within a unified framework. While SigLIP2 [40] also explores combining VL, SSL, and grounding-based self-training [41], it lacks systematic analyses of how task composition and scaling affect learned representations. In contrast, we conduct detailed studies across task diversity, data scale, and model size, revealing several novel insights—for instance, depth supervision provides strong benefits for general representation learning.

### 3. Preliminary

Our goal is to learn a unified visual representation that supports a broad spectrum of visual understanding tasks via large-scale, multi-source supervision. We begin by introducing the notations and key components used throughout the paper, covering both the shared architecture and the heterogeneous annotations that supervise it.

**Architecture.** At the core of our framework is a shared Vision Transformer (ViT) [9]  $f_\theta$  that maps an input image  $v_i \in \mathbb{R}^{H \times W \times 3}$  to multi-layer patch features:

$$\{\mathbf{z}_i^{(1)}, \dots, \mathbf{z}_i^{(L)}\} = f_\theta(v_i), \quad \mathbf{z}_i^{(l)} \in \mathbb{R}^{N \times D},$$

where  $L$  is the number of layers,  $N$  the number of patches, and  $D$  the feature dimension. For brevity, we denote the final layer representation as  $\mathbf{z}_i := \mathbf{z}_i^{(L)}$ . For tasks requiring a global image-level representation, we apply attentive pooling [49] to the final patch features:  $\mathbf{v}_i = \text{Pool}(\mathbf{z}_i) \in \mathbb{R}^D$ .

Simultaneously, a text encoder  $g_\phi$  processes natural language inputs. To enable cross-modal alignment,  $g_\phi$  maps text  $t_i$  into a joint latent space shared with the pooled visual features, producing the text embedding  $\mathbf{t}_i = g_\phi(t_i) \in \mathbb{R}^D$ .

**Data.** We consider a pretraining corpus  $\mathcal{D} = \{(v_i, a_i)\}$ , where each image  $v_i$  is paired with automatically acquired annotations  $a_i$  that provide semantic, spatial, and geometric signals: (i) A **caption**  $t_i$  capturing the global semantics of the image, used for vision-language contrastive learning; (ii) **Region-text pairs**  $\{(b_{ij}, r_{ij})\}$  where  $b_{ij}$  and  $r_{ij}$  denote the  $j$ -th bounding box and its entity name. These pairs are obtained by extracting salient entities from each image using RAM++[17], and then prompting the open-vocabulary detector OWLv2-Base[29] to localize the referred regions; thus enabling large-scale grounding supervision without human annotations; (iii) A **relative depth map**  $d_i \in \mathbb{R}^{H \times W}$  that encodes the per-pixel depth, produced by the Depth-Anything-V2-Large model [45].

These heterogeneous annotations, derived entirely from web data and off-the-shelf specialist models, provide a rich supervisory signal for studying the effectiveness of large-scale multi-task representation learning.

## 4. Multi-task Visual Representation Learning

This section details **MTV**, a principled multi-task visual representation learning framework. MTV optimizes a shared encoder across three complementary supervision paradigms: (i) vision-language (VL) contrastive learning for global semantic alignment, (ii) self-supervised learning (SSL) to induce local structural invariances and regularize feature geometry, and (iii) dense supervision to capture fine-grained spatial structure. We elaborate on each supervisory component and the training objective below.

### 4.1. Global Semantic Supervision

We adopt vision–language contrastive learning to provide global semantic supervision by aligning image and text embeddings at the instance level. This objective enables the model to learn high-level semantic representations from noisy, large-scale web data.

Given a batch of image–text pairs  $\mathcal{B} = \{(v_i, t_j)\}_{i=1}^B$ , the visual and textual embeddings  $\mathbf{v}_i$  and  $\mathbf{t}_i$  are obtained using the visual encoder and text encoder, as defined in Section 3. We adopt the sigmoid-based objective introduced by SigLIP [49], which treats the alignment task as a dense pairwise binary classification problem:

$$\mathcal{L}_{\text{VL}} = -\frac{1}{B} \sum_{i=1}^B \sum_{j=1}^B \log \frac{1}{1 + e^{y_{ij}(-\tau \mathbf{v}_i \cdot \mathbf{t}_j + \beta)}}, \quad (1)$$

where  $y_{ij} = 1$  if  $(v_i, t_j)$  is a matched pair and  $-1$  otherwise. The logit scale  $\tau$  and bias  $\beta$  are learnable parameters initialized from  $\log 10$  and  $-10$ , respectively, as in [49]. Unlike the softmax-based contrastive loss [33], the sigmoid objective decouples the batch size from the normalization, leading to more stable gradients at scale.

To support large-scale distributed training, SigLIP originally employs a cyclic rotation-based protocol to avoid large collective communication. However, in our framework, we observe that the communication overhead of text embeddings is negligible relative to the computational cost of the shared multi-task backbone. Therefore, we utilize a more direct and implementation-efficient alternative: we synchronize textual embeddings across all devices using a differentiable `all_gather`<sup>1</sup> operation. This preserves the mathematical correctness of Eq. 1 while facilitating easier integration within a multi-task pipeline.

### 4.2. Self-Supervised Objectives

While vision–language supervision captures global semantics, it provides limited guidance for learning locally consistent features. To complement the VL objective, we incorpo-

<sup>1</sup>`all_gather` is a collective communication primitive that synchronizes and collects tensors from all devices. We use a differentiable version of it that supports gradient backpropagation through  $\mathbf{t}_j$ .

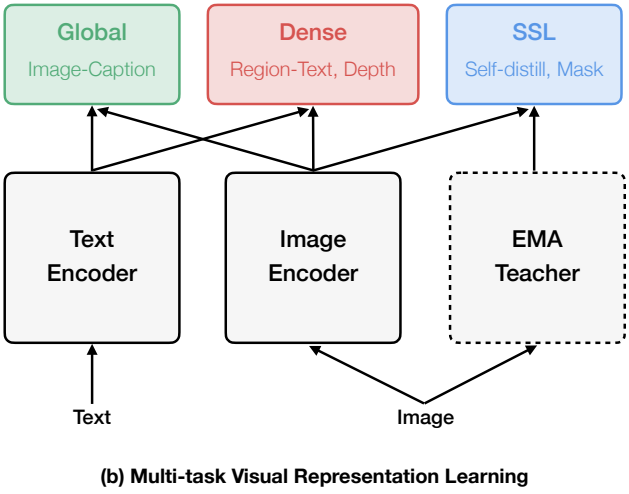


Figure 2. **Overview of our MTV framework.** (a) Each image is paired with a web-crawled caption, and augmented with pseudo region–text pairs and relative depth maps generated by teacher models. (b) MTV jointly learns from three complementary supervision types: **Global** (image–caption contrast), **Dense** (region–text alignment, depth), and **SSL** (self-distillation, masked feature prediction). A shared image encoder is optimized together with a text encoder and an EMA teacher.

rate two self-supervised tasks within a teacher-student distillation framework: (i) local-to-global self-distillation [5] and (ii) masked feature prediction [51].

Following the architecture in DINOv2 [32] and TIPS [27], our student network comprises the visual encoder  $f_\theta$  and separate MLP projection heads for each SSL task to mitigate gradient interference. The teacher network is maintained as an Exponential Moving Average (EMA) of the student, providing stable targets throughout pretraining.

**Local-to-Global Self-distillation** encourages spatial consistency by aligning the representations of local and global views. For each image  $v_i$ , the student processes  $M = 6$  local crops to produce their global embeddings  $\{\mathbf{v}_{i,m}\}_{m=1}^M$ , which are then projected into “prototype scores”  $\{\mathbf{p}_i^m\}_{m=1}^M$  by the student MLP. Simultaneously, the teacher processes a larger, global crop to produce the target scores  $\hat{\mathbf{p}}_i$ . The student is trained to match the teacher’s distribution using a temperature-scaled KL divergence:

$$\mathcal{L}_{\text{distill}} = - \sum_i^B \sum_m^M \text{KL} \left( \text{softmax} \left( \frac{\hat{\mathbf{p}}_i - \mathbf{c}}{\tau_t} \right) \middle\| \text{softmax} \left( \frac{\mathbf{p}_i^m}{\tau_s} \right) \right),$$

where  $\tau_t$  and  $\tau_s$  are the teacher and student temperatures for score sharpening, and  $\mathbf{c}$  is an EMA-updated centering variable that prevents collapsing to a trivial solution by encouraging a uniform distribution across prototypes.

**Masked Feature Prediction** focuses on capturing fine-grained spatial dependencies. We randomly mask 50% of the patches in  $v_i$  and replace them with a learnable mask token. The student encodes the masked input into prototype scores  $\{\mathbf{p}_i^j\}$ , while the teacher processes the original

unmasked image to provide target scores  $\{\hat{\mathbf{p}}_i^j\}$  for the corresponding masked locations  $j$ . The student is trained to match the teacher’s distributions at these masked locations:

$$\mathcal{L}_{\text{mask}} = - \sum_i^B \sum_{j \in \text{masked}} \text{KL} \left( \text{softmax} \left( \frac{\hat{\mathbf{p}}_i^j - \mathbf{c}}{\tau_t} \right) \middle\| \text{softmax} \left( \frac{\mathbf{p}_i^j}{\tau_s} \right) \right),$$

thereby forcing the encoder to model long-range spatial regularities from incomplete inputs.

Following [32], we further include the KoLeo regularizer [36] to promote a more uniform feature distribution within each batch. The total SSL objective is defined as:

$$\mathcal{L}_{\text{SSL}} = \mathcal{L}_{\text{distill}} + \lambda_{\text{mask}} \times \mathcal{L}_{\text{mask}} + \lambda_{\text{koleo}} \times \mathcal{L}_{\text{koleo}}, \quad (2)$$

where  $\lambda_{\text{mask}}=2$  and  $\lambda_{\text{koleo}}=0.1$  as in [27, 32]. By integrating  $\mathcal{L}_{\text{SSL}}$  with the global VL loss, the model learns representations that are both semantically rich and spatially grounded.

### 4.3. Dense Structured Supervision

While VL and SSL provide semantic and structural regularities, they often lack the explicit spatial precision required for dense downstream tasks. To bridge this gap, we incorporate dense structured supervision by distilling knowledge from high-capacity expert models into our shared encoder. Concretely, we introduce two complementary objectives: (i) region-level grounding for object-level semantics and (ii) per-pixel depth regression for fine-grained geometry.

**Region-level Grounding.** To enforce spatial grounding, we incorporate regional-textual correspondences. For each image  $v_i$ , we sample up to four region–text pseudo-labels to

balance supervision density and computational cost. The visual and textual inputs are encoded into patch-level features  $\mathbf{z}_i$  and region text embeddings  $\mathbf{t}_{ij}$ , respectively. Following CLOC [6], we utilize the Soft Region Aggregation mechanism to handle potential misalignments in pseudo-labels. Specifically, a lightweight Transformer layer processes the patch-level features  $\mathbf{z}_i$ , conditioned on the positional encodings derived from each bounding box. This learnable attention allows the model to adaptively integrate context beyond rigid box boundaries, mitigating noise in pseudo labels. The resulting soft region embeddings  $\mathbf{z}_{ij}$  are aligned with their corresponding text embeddings  $\mathbf{t}_{ij}$  using the sigmoid contrastive loss (Eq. 1), yielding the grounding loss  $\mathcal{L}_{\text{ground}}$ .

**Pixel-level Geometric Supervision.** To capture dense geometric priors, we incorporate monocular depth estimation supervised by high-fidelity pseudo labels. We attach a lightweight DPT head [34] to the shared visual encoder, which aggregates multi-layer features  $\{\mathbf{z}_i^{(l)}\}_{l \in \mathcal{S}}$  from selected ViT layers to predict a dense depth map  $\hat{d}_i \in \mathbb{R}^{H \times W}$ . The prediction is supervised using a combination of scale- and shift-invariant loss alongside a multi-scale gradient loss from MiDaS [3], jointly denoted as  $\mathcal{L}_{\text{depth}}$ . To mitigate the influence of potential artifacts in pseudo labels, we adopt a top- $K$  denoising strategy, discarding the highest 10% of per-pixel losses within each sample during training. This encourages the encoder to prioritize high-confidence geometric structures, providing a structural anchor that complements the global semantic objectives. Detailed loss formulations are provided in Section A.2.

By unifying region-level semantics and pixel-level geometry, the total dense supervision loss is defined as:

$$\mathcal{L}_{\text{Dense}} = \mathcal{L}_{\text{ground}} + \mathcal{L}_{\text{depth}}. \quad (3)$$

#### 4.4. Joint Optimization

We optimize the shared visual encoder by jointly minimizing a multi-task objective that integrates the VL, SSL, and dense supervision signals introduced in Eqs. (1)–(3):

$$\mathcal{L}_{\text{total}} = \mathcal{L}_{\text{VL}} + \mathcal{L}_{\text{SSL}} + \mathcal{L}_{\text{Dense}}.$$

Notably, we find uniform loss weighting yields stable convergence and competitive performance. Consequently, no exhaustive hyperparameter tuning is performed. This stability suggests a high degree of task synergy within the MTV framework. As shown in Figure 2, each training sample is fully annotated with a caption, open-vocabulary grounding, and a relative depth map. By leveraging expert models to synthesize these structured pseudo-labels for every image in our pretraining corpus, we eliminate the need for complex task-specific sampling. This unified training interface allows the shared encoder to efficiently internalize the full spectrum of visual information in a single pass.

## 5. Experiments

### 5.1. Training Details

**Architecture.** We evaluate our MTV framework using ViT-B/16-224 and ViT-L/16-256 backbones, following the SigLIP [49] architecture and its text tokenizer. To accommodate the multi-task nature of MTV, we attach lightweight heads for SSL (MLP heads), grounding (Transformer aggregator), and depth estimation (DPT head). Table 1 summarizes the incremental cost of each task, while architectural specifications are detailed in Section A.2.

**Training Data Curation.** All experiments are conducted on the DataComp dataset [12]. We crawled 200 million raw image–text pairs and applied a filtering pipeline. We discard images with a shorter side  $< 224$  pixels and downsample high-resolution images to a maximum dimension of 1024 pixels while maintaining aspect ratios. This filtering removes low-information outliers and ensures that the “expert” models—OWLv2 and Depth Anything V2—operate within their optimal receptive fields. We then apply the pseudo-labeling procedure described in Section 3, resulting in 100 million “fully-labeled” samples, each containing a caption, region–text pairs, and a relative depth map.

**Optimization Configurations.** All experiments are conducted on NVIDIA H200 GPUs. We investigate the scaling behavior of MTV at three data scales: 10M, 50M, and 100M samples. The 10M and 50M data scales are used primarily for ablation studies and are trained for 20 and 10 epochs, respectively, with a global batch size of 4k. Our full-scale 100M model is trained for 32 epochs with a global batch size of 8k, following the standard CLIP [33] protocol for fair comparison. We use the AdamW optimizer with a learning rate of  $5 \times 10^{-4}$ , no weight decay, and a linear warmup over the first 1k steps. Training utilizes BF16 mixed precision for efficiency, with the exception of the DPT depth head, which is kept in FP32 to ensure numerical stability for regressing continuous geometric values.

### 5.2. Evaluation Details

We evaluate the learned representations across a broad set of downstream tasks spanning global-semantic understanding and fine-grained spatial reasoning. As summarized in Table 2, each task is assessed on one or more representative benchmarks. Below, we outline the setup for each task.

**Zero-shot Image Classification.** We report Top-1 accuracy on the ImageNet-1k [35] validation set using the standard prompt-based zero-shot protocol.

**Zero-shot Retrieval.** For cross-modal alignment, we evaluate image-to-text ( $I \rightarrow T$ ) and text-to-image retrieval ( $T \rightarrow I$ ) on COCO [8], reporting the Recall@1 metric.

**MLLM VQA.** To assess the quality of our visual features for higher-level reasoning, we integrate the frozen

Table 1. **Training Cost** for a ViT-B/16 model under different task combinations. (Numbers in parentheses) indicate the increase over the previous row. \* The EMA teacher used in SSL is frozen.

Training Tasks	Trainable Params.	Train Time
VL	203.2 M	1.0×
VL + SSL*	232.6 M (+29.4 M)	1.2× (+20%)
VL + SSL + Ground.	239.7 M (+7.1 M)	1.5× (+25%)
VL + SSL + Ground. + Depth	250.3 M (+10.6 M)	1.7× (+13%)

Table 2. **Summary of evaluation benchmarks.**

Task	Metric	Benchmark
<i>Global Semantic Understanding</i>		
Zero-shot Classification	Top-1 Acc.	ImageNet-1k
Zero-shot Retrieval	Recall@1	COCO
<i>Fine-grained Spatial Reasoning</i>		
Semantic Segmentation	mIoU	ADE20k
Geometric Correspondence	Avg. Recall	NAVI
Semantic Correspondence	Avg. Recall	SPair
Monocular Depth	RMSE	NYUv2

MTV encoder into the TinyLLaVA framework [20] with a Qwen2.5-3B language model. Following the standard two-stage recipe, we train the model on LLaVA-558K, followed by supervised fine-tuning on LLaVA-NEXT-779K [24]. Evaluation is conducted on three vision-centric VQA benchmarks categorized by [38], including MMVP [39], CVBench [38], and RealWorldQA [42]. We report the average score across these benchmarks.

**Semantic Segmentation.** We evaluate on ADE20k [50] using a frozen visual encoder and a linear classification head to predict per-patch semantic labels. Training runs for 40k steps with batch size 32, learning rate 4e-5, and  $576 \times 576$  input resolution. Performance is measured by mean Intersection-over-Union (mIoU).

**Geometric and Semantic Correspondence.** To investigate the model’s 3D awareness, we utilize the Probe3D framework [10]. We assess *geometric correspondence* on NAVI [18], which requires matching pixels originating from the same 3D point across different viewpoints. We further evaluate *semantic correspondence* on SPair [28], testing the alignment of semantically similar parts across diverse instances. Both tasks are measured using Average Recall across various viewpoints or distances.

**Monocular Depth Estimation.** Following [32, 40, 48], we concatenate the global token to each patch token output by the frozen visual encoder, and train a linear head to predict depth across 256 discretized bins. A classification loss is used during training on NYUv2 [37], with evaluation on its test set. See [48] for more implementation details.

### 5.3. Ablations and Analysis

We organize our analysis around three core questions.

#### Q1: Marginal Gains and Task Contributions.

We first examine whether integrating heterogeneous objectives is consistently beneficial. Table 3 presents the incremental performance along a principled task expansion path: VL  $\rightarrow$  +SSL  $\rightarrow$  +Ground.  $\rightarrow$  +Depth.

Across data and model scales, performance almost always improves monotonically at every step. **Absolute Gain**  $\Delta$  highlights that the full multi-task framework is strictly better than the VL-only baseline. This demonstrates that rather than interference, these objectives provide complementary supervision that enriches the shared representation.

We also observe distinct roles for each objective: (i) SSL acts as a powerful general-purpose enhancer, significantly lifting both semantic (+14.4% on IN-1k for ViT-L/10M) and spatial benchmarks (+10.4 on ADE20k). This suggests that local structural regularities provide a necessary geometric scaffold for global semantics. (ii) Since grounding serves as a fine-grained vision-language signal, it not only boosts spatial tasks but also provides benefits to global multimodal understanding, such as the +3.8 R@1 gain in COCO I $\rightarrow$ T retrieval. (iii) Adding depth supervision consistently yields the final refinement for pixel-level tasks, improving NYUv2 by up to 0.051 in the ViT-L/50M setting.

While the gains exhibit diminishing marginal returns as the representation nears saturation, the large initial jump from SSL should be interpreted with caution. These relative improvements are partially a consequence of the chosen expansion order and the inherent spatial sparsity of the VL-only baseline. Nevertheless, the consistent positive deltas verify the robustness of the joint optimization.

#### Q2: Synergy vs. Interference among Objectives.

We further investigate how heterogeneous objectives interact during joint optimization. To quantify their complementarity, we define a *Task Synergy* metric as:

$$\text{Synergy}(A, B) = \frac{\Delta AB - \max(\Delta A, \Delta B)}{\max(\Delta A, \Delta B)}, \quad (4)$$

where  $\Delta A$  and  $\Delta B$  denote the individual performance gains over the VL baseline, and  $\Delta AB$  is the gain achieved by their combination. Intuitively, a positive score indicates that the tasks are mutually beneficial, providing gains beyond those attainable by the superior individual task alone.

As shown in Table 4, all task pairs exhibit positive average synergy across data and model scales, typically ranging from 20% to 50%. This empirically confirms that the objectives are fundamentally complementary rather than interfering with MTV. Task pairs involving grounding show particularly robust synergy, reinforcing our argument that region–text alignment serves as a critical bridge between high-level semantics and fine-grained spatial structures.

Table 3. **Task Scaling Effects** across model sizes and data scales. (Numbers in parentheses) indicate the incremental increase over the previous row, while **Absolute Gain  $\Delta$**  denotes the overall performance improvement of full multi-task training over the VL-only baseline.

ViT	Data	Training Tasks	IN-1k	COCO	VQA	ADE20k	NAVI	SPair	NYUv2	
			Acc.	T $\rightarrow$ I	I $\rightarrow$ T	Score	mIoU	Recall	Recall	RMSE $\downarrow$
B/16	10M	VL	36.2	14.8	21.9	41.1	27.5	39.5	17.0	0.643
		VL + SSL	43.7 (+7.5)	19.7 (+4.9)	28.6 (+6.7)	43.1 (+2.0)	36.2 (+8.7)	41.5 (+2.0)	21.1 (+4.1)	0.568 (-.075)
		VL + SSL + Ground.	49.0 (+5.3)	23.5 (+3.8)	33.9 (+5.3)	43.2 (+0.1)	39.5 (+3.3)	43.3 (+1.8)	22.4 (+1.3)	0.537 (-.031)
		VL + SSL + Ground. + Depth	49.7 (+0.7)	23.9 (+0.4)	34.1 (+0.2)	43.4 (+0.2)	41.7 (+2.2)	43.6 (+0.3)	22.8 (+0.4)	0.512 (-.025)
		<b>Absolute Gain <math>\Delta</math></b>	<b>+13.5</b>	<b>+9.1</b>	<b>+12.2</b>	<b>+2.3</b>	<b>+14.2</b>	<b>+4.1</b>	<b>+5.8</b>	<b>-0.131</b>
B/16	50M	VL	55.7	28.2	43.0	42.2	32.2	39.8	18.0	0.604
		VL + SSL	61.4 (+5.7)	32.4 (+4.2)	48.0 (+5.0)	44.7 (+2.5)	39.9 (+7.7)	40.4 (+0.6)	22.7 (+4.7)	0.556 (-.048)
		VL + SSL + Ground.	62.9 (+1.5)	34.7 (+2.3)	50.7 (+2.7)	45.1 (+0.4)	43.0 (+3.1)	43.8 (+3.4)	25.4 (+2.7)	0.513 (-.043)
		VL + SSL + Ground. + Depth	62.9	35.0 (+0.3)	50.5 (-0.2)	45.8 (+0.7)	43.7 (+0.7)	44.1 (+0.3)	24.5 (-0.9)	0.482 (-.031)
		<b>Absolute Gain <math>\Delta</math></b>	<b>+7.2</b>	<b>+6.8</b>	<b>+7.5</b>	<b>+3.6</b>	<b>+11.5</b>	<b>+4.3</b>	<b>+6.5</b>	<b>-0.122</b>
L/16	10M	VL	35.0	14.9	21.6	39.0	30.0	40.1	18.1	0.630
		VL + SSL	49.4 (+14.4)	23.7 (+8.8)	34.0 (+12.4)	42.1 (+3.1)	40.4 (+10.4)	43.4 (+3.3)	25.6 (+7.5)	0.535 (-.095)
		VL + SSL + Ground.	53.4 (+4.0)	25.6 (+1.9)	37.8 (+3.8)	43.7 (+1.6)	43.6 (+3.2)	44.3 (+0.9)	27.0 (+1.4)	0.498 (-.037)
		VL + SSL + Ground. + Depth	54.3 (+0.9)	26.6 (+1.0)	38.6 (+0.8)	44.3 (+0.6)	45.6 (+2.0)	46.2 (+1.9)	27.5 (+0.5)	0.455 (-.043)
		<b>Absolute Gain <math>\Delta</math></b>	<b>+19.3</b>	<b>+11.7</b>	<b>+17.0</b>	<b>+5.3</b>	<b>+15.6</b>	<b>+6.1</b>	<b>+9.4</b>	<b>-0.175</b>
L/16	50M	VL	60.8	31.1	46.3	43.3	37.3	39.9	19.8	0.575
		VL + SSL	65.4 (+4.6)	34.5 (+3.4)	48.0 (+1.7)	44.9 (+1.6)	45.5 (+8.2)	43.2 (+3.3)	27.3 (+7.5)	0.501 (-.074)
		VL + SSL + Ground.	67.6 (+2.2)	37.4 (+2.9)	51.5 (+3.5)	45.9 (+1.0)	47.2 (+1.7)	43.7 (+0.5)	28.1 (+0.8)	0.472 (-.029)
		VL + SSL + Ground. + Depth	67.9 (+0.3)	37.3 (-0.1)	52.3 (+0.8)	45.9	49.1 (+1.9)	45.9 (+2.2)	29.7 (+1.6)	0.421 (-.051)
		<b>Absolute Gain <math>\Delta</math></b>	<b>+7.1</b>	<b>+6.2</b>	<b>+6.0</b>	<b>+2.6</b>	<b>+11.8</b>	<b>+6.0</b>	<b>+9.9</b>	<b>-0.154</b>

Table 4. **Task Synergy (%)** computed as Equation 4, measuring the relative gain from combining two tasks beyond the larger of their individual improvements over the VL-only baseline. \*COCO is short for COCO I $\rightarrow$ T retrieval.

ViT	Data	Baseline	TaskA	TaskB	Synergy (%)						
					IN-1k	COCO*	ADE20k	NAVI	SPair	NYUv2	Average
B/16	10M	VL	SSL	Ground.	62.0	64.4	37.9	72.7	31.7	40.8	51.7
			SSL	Depth	50.7	41.8	31.0	-10.0	26.8	56.6	32.9
			Depth	Ground.	22.8	27.4	33.8	36.4	51.5	56.2	38.1
B/16	50M	VL	SSL	Ground.	26.3	54.0	40.3	100.0	57.4	44.4	53.7
			SSL	Depth	8.8	4.0	27.3	75.0	61.7	29.0	34.3
			Depth	Ground.	2.6	26.3	40.7	87.5	78.8	19.4	42.6
L/16	10M	VL	SSL	Ground.	27.8	30.6	30.8	27.3	18.7	38.9	29.0
			SSL	Depth	17.4	21.8	27.9	24.2	24.0	53.6	28.1
			Depth	Ground.	9.6	3.5	32.0	42.9	0.0	12.5	16.7
L/16	50M	VL	SSL	Ground.	47.8	33.8	30.7	21.8	10.7	39.2	30.7
			SSL	Depth	43.5	92.0	19.5	9.1	-34.7	4.6	22.3
			Depth	Ground.	45.5	33.3	33.3	29.4	17.9	18.5	29.7

We also observe distinct scaling trends between model and data scales: For the B/16 model, increasing data from 10M to 50M samples leads to more stable and stronger synergy. While synergy remains positive for the larger L/16 model, the relative scores are generally lower compared to B/16. This is expected as higher-capacity VL baselines naturally leave less relative headroom for additional supervision, even as absolute performance continues to rise.

### Q3: Scaling Effects across Data and Model Capacity.

We finally investigate how MTV scales with data size and model capacity. As illustrated in Figure 3, scaling the data yields broadly monotonic improvements. Notably, our

ViT-Base model trained on only 100M samples consistently outperforms the CLIP-Base baseline, which was trained on 400M samples. This demonstrates that multi-task supervision can be more data-efficient than pure VL pretraining for building versatile visual encoders.

However, the scaling behavior is not uniform across tasks. Geometric and semantic correspondence saturates and begins to decline once the number of seen samples exceeds 1B. This suggests that correspondence tasks may not benefit from naive data scaling alone and likely require more targeted architectural designs or supervision.

Moreover, model scaling from B/16 to L/16 (Table 3,

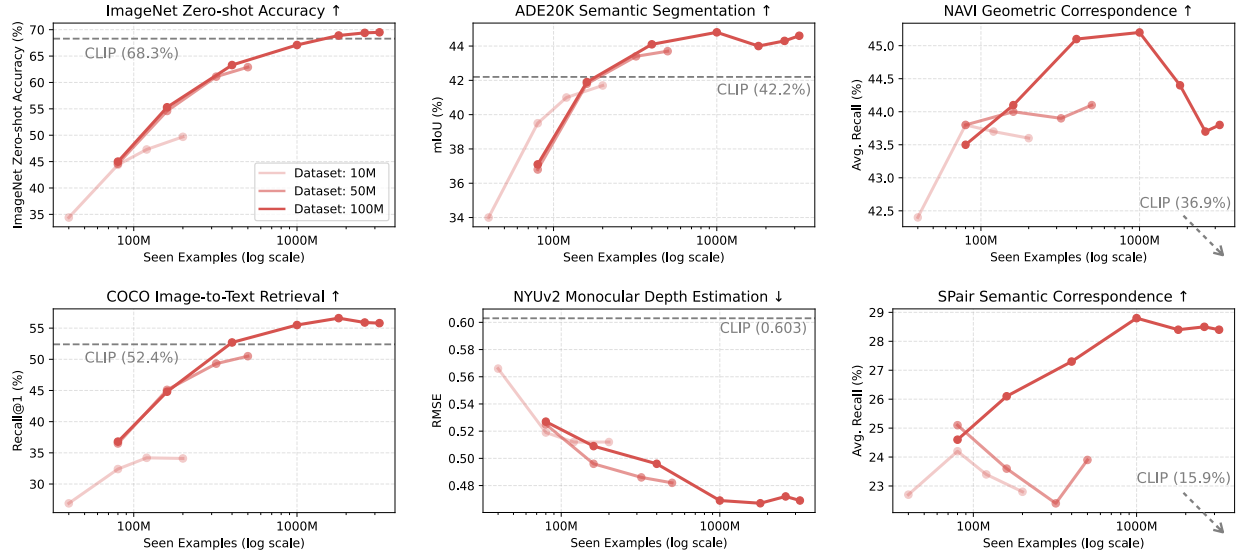


Figure 3. **Data scaling behavior of multi-task visual pretraining.** ViT-Base models are trained with 10M, 50M, and 100M samples under our multi-task setting. CLIP-Base [33] is shown as gray dashed line. Lower ↓ is better for NYUv2; higher ↑ is better elsewhere.

Table 5. Comprehensive comparisons with large-scale VLMs.

ViT	Model	Data	IN-1k		COCO		VQA		ADE20K		NAVI		SPair		NYUv2	
			Acc.	T→I	I→T	Score	mIoU	Recall	Recall	RMSE ↓						
B/16	CLIP [33]	400M	68.3	33.1	52.4	44.8	42.2	36.9	15.9	0.603						
	SigLIP [49]	10B	76.2	47.2	64.5	47.7	45.1	38.5	17.3	0.615						
	SigLIP2 [40]	10B	<b>78.2</b>	<b>52.1</b>	<b>68.9</b>	<b>48.1</b>	<b>46.0</b>	38.0	20.8	0.562						
	<b>MTV</b>	100M	69.5	41.2	57.1	45.6	44.6	<b>43.8</b>	<b>28.4</b>	<b>0.469</b>						
L/14	CLIP [33]	400M	75.5	36.5	56.3	46.5	46.2	36.0	20.5	0.588						
	SigLIP [49]	10B	80.5	51.2	69.6	48.3	47.7	38.8	19.7	0.550						
	SigLIP2 [40]	10B	<b>82.5</b>	<b>54.7</b>	<b>71.5</b>	<b>52.5</b>	<b>51.6</b>	43.2	29.9	0.484						
	<b>MTV</b>	100M	75.2	43.0	58.1	47.6	48.2	<b>45.0</b>	<b>30.1</b>	<b>0.414</b>						

Table 5) improves performance across tasks under the same data scale, narrowing the gap to larger VL-only baselines while preserving strong spatial understanding.

Overall, these findings indicate that while MTV scales favorably, certain geometric tasks remain a bottleneck, suggesting that the path to general-purpose vision models involves more than simply increasing data and model size.

#### 5.4. Comparison with State-of-the-art

We comprehensively compare MTV with representative vision–language models (VLMs) in Table 5.

On **global semantic tasks** such as classification, retrieval, and VQA, our models consistently outperform CLIP, despite using only one-quarter of its training data. As expected, our models lag behind SigLIP and SigLIP2, which are trained on 100× more data, but the performance gap remains modest given the vast scale difference.

On **fine-grained spatial tasks**, the advantages of MTV are most prominent. Ours tail SigLIP and SigLIP2 on semantic segmentation, while achieving clearly better performance on correspondence and depth estimation.

Taken together, these results demonstrate that multi-task training offers a compelling and scalable alternative to purely vision–language or self-supervised pretraining for general-purpose visual representation learning.

## 6. Conclusion

In this work, we revisit large-scale multi-task training as a unified framework for learning general-purpose visual representations. By jointly optimizing vision–language contrastive, self-supervised, and dense pseudo-labeled objectives, our model, MTV, acquires strong semantic and geometric understanding within a single encoder. Across extensive experiments, we demonstrate that multi-task supervision leads to steadily improving performance as more tasks are incorporated, exhibiting clear task synergy and favorable data- and model-scaling behavior. These findings suggest that multi-task pretraining, fueled by high-quality pseudo-supervision, provides an effective and data-efficient route toward universal visual foundation models for broad visual perception and reasoning tasks.

## References

[1] Josh Achiam, Steven Adler, Sandhini Agarwal, Lama Ahmad, Ilge Akkaya, Florencia Leoni Aleman, Diogo Almeida, Janko Altenschmidt, Sam Altman, Shyamal Anadkat, et al. Gpt-4 technical report. *arXiv preprint arXiv:2303.08774*, 2023. 1

[2] Mahmoud Assran, Quentin Duval, Ishan Misra, Piotr Bojanowski, Pascal Vincent, Michael Rabbat, Yann LeCun, and Nicolas Ballas. Self-supervised learning from images with a joint-embedding predictive architecture. In *CVPR*, 2023. 2

[3] Reiner Birk, Diana Wofk, and Matthias Müller. Midas v3. 1-a model zoo for robust monocular relative depth estimation. *arXiv preprint arXiv:2307.14460*, 2023. 5, 1, 2

[4] Tom Brown, Benjamin Mann, Nick Ryder, Melanie Subbiah, Jared D Kaplan, Prafulla Dhariwal, Arvind Neelakantan, Pranav Shyam, Girish Sastry, Amanda Askell, et al. Language models are few-shot learners. In *NeurIPS*, 2020. 1

[5] Mathilde Caron, Hugo Touvron, Ishan Misra, Hervé Jégou, Julien Mairal, Piotr Bojanowski, and Armand Joulin. Emerging properties in self-supervised vision transformers. In *ICCV*, 2021. 1, 2, 4

[6] Hong-You Chen, Zhengfeng Lai, Haotian Zhang, Xinze Wang, Marcin Eichner, Keen You, Meng Cao, Bowen Zhang, Yafei Yang, and Zhe Gan. Contrastive localized language-image pre-training. In *ICML*, 2025. 5, 1

[7] Ting Chen, Simon Kornblith, Mohammad Norouzi, and Geoffrey Hinton. A simple framework for contrastive learning of visual representations. In *ICML*, 2020. 1

[8] Xinlei Chen, Hao Fang, Tsung-Yi Lin, Ramakrishna Vedantam, Saurabh Gupta, Piotr Dollár, and C Lawrence Zitnick. Microsoft coco captions: Data collection and evaluation server. *arXiv preprint arXiv:1504.00325*, 2015. 5

[9] Alexey Dosovitskiy, Lucas Beyer, Alexander Kolesnikov, Dirk Weissenborn, Xiaohua Zhai, Thomas Unterthiner, Mostafa Dehghani, Matthias Minderer, Georg Heigold, Sylvain Gelly, Jakob Uszkoreit, and Neil Houlsby. An image is worth 16x16 words: Transformers for image recognition at scale. In *ICLR*, 2021. 3

[10] Mohamed El Banani, Amit Raj, Kevis-Kokitsi Maninis, Abhishek Kar, Yuanzhen Li, Michael Rubinstein, Deqing Sun, Leonidas Guibas, Justin Johnson, and Varun Jampani. Probing the 3d awareness of visual foundation models. In *CVPR*, 2024. 1, 2, 6

[11] Lijie Fan, Dilip Krishnan, Phillip Isola, Dina Katabi, and Yonglong Tian. Improving clip training with language rewrites. In *NeurIPS*, 2023. 2

[12] Samir Yitzhak Gadre, Gabriel Ilharco, Alex Fang, Jonathan Hayase, Georgios Smyrnis, Thao Nguyen, Ryan Marten, Mitchell Wortsman, Dhruba Ghosh, Jieyu Zhang, et al. Dat-acomp: In search of the next generation of multimodal datasets. In *NeurIPS*, 2023. 5, 1

[13] Andreas Geiger, Philip Lenz, and Raquel Urtasun. Are we ready for autonomous driving? the kitti vision benchmark suite. In *CVPR*, 2012. 2

[14] Golnaz Ghiasi, Barret Zoph, Ekin D Cubuk, Quoc V Le, and Tsung-Yi Lin. Multi-task self-training for learning general representations. In *ICCV*, 2021. 2

[15] Kaiming He, Haoqi Fan, Yuxin Wu, Saining Xie, and Ross Girshick. Momentum contrast for unsupervised visual representation learning. In *CVPR*, 2020. 1

[16] Kaiming He, Xinlei Chen, Saining Xie, Yanghao Li, Piotr Dollár, and Ross Girshick. Masked autoencoders are scalable vision learners. In *CVPR*, 2022. 1, 2

[17] Xinyu Huang, Yi-Jie Huang, Youcai Zhang, Weiwei Tian, Rui Feng, Yuejie Zhang, Yanchun Xie, Yaqian Li, and Lei Zhang. Open-set image tagging with multi-grained text supervision. *arXiv preprint arXiv:2310.15200*, 2023. 3, 1

[18] Varun Jampani, Kevis-Kokitsi Maninis, Andreas Engelhardt, Arjun Karpur, Karen Truong, Kyle Sargent, Stefan Popov, André Araújo, Ricardo Martin Bruxalla, Kaushal Patel, et al. Navi: Category-agnostic image collections with high-quality 3d shape and pose annotations. In *NeurIPS*, 2023. 6

[19] Chao Jia, Yafei Yang, Ye Xia, Yi-Ting Chen, Zarana Parekh, Hieu Pham, Quoc Le, Yun-Hsuan Sung, Zhen Li, and Tom Duerig. Scaling up visual and vision-language representation learning with noisy text supervision. In *ICML*, 2021. 1, 2

[20] Junlong Jia, Ying Hu, Xi Weng, Yiming Shi, Miao Li, Xingjian Zhang, Baichuan Zhou, Ziyu Liu, Jie Luo, Lei Huang, and Ji Wu. Tinyllava factory: A modularized codebase for small-scale large multimodal models. *arXiv preprint arXiv:2405.11788*, 2024. 6

[21] Jared Kaplan, Sam McCandlish, Tom Henighan, Tom B Brown, Benjamin Chess, Rewon Child, Scott Gray, Alec Radford, Jeffrey Wu, and Dario Amodei. Scaling laws for neural language models. *arXiv preprint arXiv:2001.08361*, 2020. 1

[22] Bingxin Ke, Anton Obukhov, Shengyu Huang, Nando Metzger, Rodrigo Caye Daudt, and Konrad Schindler. Repurposing diffusion-based image generators for monocular depth estimation. In *CVPR*, 2024. 2

[23] Zhengfeng Lai, Haotian Zhang, Bowen Zhang, Wentao Wu, Haoping Bai, Aleksei Timofeev, Xianzhi Du, Zhe Gan, Jiu-long Shan, Chen-Nee Chuah, et al. Veclip: Improving clip training via visual-enriched captions. In *ECCV*, 2024. 2

[24] Haotian Liu, Chunyuan Li, Yuheng Li, Bo Li, Yuanhan Zhang, Sheng Shen, and Yong Jae Lee. Llava-next: Improved reasoning, ocr, and world knowledge, 2024. 6

[25] Yanqing Liu, Xianhang Li, Zeyu Wang, Bingchen Zhao, and Cihang Xie. Clips: An enhanced clip framework for learning with synthetic captions. *arXiv preprint arXiv:2411.16828*, 2024. 2

[26] Yiming Liu, Yuhui Zhang, Dhruba Ghosh, Ludwig Schmidt, and Serena Yeung-Levy. Data or language supervision: What makes CLIP better than DINO? In *EMNLP Findings*, 2025. 1

[27] Kevis-Kokitsi Maninis, Kaifeng Chen, Soham Ghosh, Arjun Karpur, Koert Chen, Ye Xia, Bingyi Cao, Daniel Salz, Guangxing Han, Jan Dlabař, et al. Tips: Text-image pre-training with spatial awareness. In *ICLR*, 2025. 2, 4

[28] Juhong Min, Jongmin Lee, Jean Ponce, and Minsu Cho. Spair-71k: A large-scale benchmark for semantic correspondence. *arXiv preprint arXiv:1908.10543*, 2019. 6

[29] Matthias Minderer, Alexey Gritsenko, and Neil Houlsby. Scaling open-vocabulary object detection. In *NeurIPS*, 2023. 2, 3, 1

[30] Norman Mu, Alexander Kirillov, David Wagner, and Saining Xie. Slip: Self-supervision meets language-image pre-training. In *ECCV*, 2022. 2

[31] Muhammad Ferjad Naeem, Yongqin Xian, Xiaohua Zhai, Lukas Hoyer, Luc Van Gool, and Federico Tombari. Silc: Improving vision language pretraining with self-distillation. In *ECCV*, 2024. 2

[32] Maxime Oquab, Timothée Darcet, Théo Moutakanni, Huy Vo, Marc Szafraniec, Vasil Khalidov, Pierre Fernandez, Daniel Haziza, Francisco Massa, Alaaeldin El-Nouby, et al. Dinov2: Learning robust visual features without supervision. *arXiv preprint arXiv:2304.07193*, 2023. 1, 2, 4, 6

[33] Alec Radford, Jong Wook Kim, Chris Hallacy, Aditya Ramesh, Gabriel Goh, Sandhini Agarwal, Girish Sastry, Amanda Askell, Pamela Mishkin, Jack Clark, et al. Learning transferable visual models from natural language supervision. In *ICML*, 2021. 1, 2, 3, 5, 8

[34] René Ranftl, Alexey Bochkovskiy, and Vladlen Koltun. Vision transformers for dense prediction. In *ICCV*, 2021. 5, 1

[35] Olga Russakovsky, Jia Deng, Hao Su, Jonathan Krause, Sanjeev Satheesh, Sean Ma, Zhiheng Huang, Andrej Karpathy, Aditya Khosla, Michael Bernstein, et al. Imagenet large scale visual recognition challenge. *IJCV*, 2015. 5

[36] Alexandre Sablayrolles, Matthijs Douze, Cordelia Schmid, and Hervé Jégou. Spreading vectors for similarity search. In *ICLR*, 2019. 4

[37] Nathan Silberman, Derek Hoiem, Pushmeet Kohli, and Rob Fergus. Indoor segmentation and support inference from rgbd images. In *ECCV*, 2012. 6, 2

[38] Peter Tong, Ellis Brown, Penghao Wu, Sanghyun Woo, Adithya Jairam Vedagiri IYER, Sai Charitha Akula, Shusheng Yang, Jihan Yang, Manoj Middepogu, Ziteng Wang, et al. Cambrian-1: A fully open, vision-centric exploration of multimodal llms. In *NeurIPS*, 2024. 1, 2, 6

[39] Shengbang Tong, Zhuang Liu, Yuexiang Zhai, Yi Ma, Yann LeCun, and Saining Xie. Eyes wide shut? exploring the visual shortcomings of multimodal llms. In *CVPR*, 2024. 1, 6

[40] Michael Tschannen, Alexey Gritsenko, Xiao Wang, Muhammad Ferjad Naeem, Ibrahim Alabdulmohsin, Nikhil Parthasarathy, Talfan Evans, Lucas Beyer, Ye Xia, Basil Mustafa, et al. Siglip 2: Multilingual vision-language encoders with improved semantic understanding, localization, and dense features. *arXiv preprint arXiv:2502.14786*, 2025. 3, 6, 8

[41] Bo Wan, Michael Tschannen, Yongqin Xian, Filip Pavetic, Ibrahim M Alabdulmohsin, Xiao Wang, André Susano Pinto, Andreas Steiner, Lucas Beyer, and Xiaohua Zhai. Locca: Visual pretraining with location-aware captioners. In *NeurIPS*, 2024. 3

[42] xAI. Grok-1.5 vision preview, 2024. 6

[43] Qizhe Xie, Minh-Thang Luong, Eduard Hovy, and Quoc V Le. Self-training with noisy student improves imagenet classification. In *CVPR*, 2020. 2

[44] Lihe Yang, Bingyi Kang, Zilong Huang, Xiaogang Xu, Jiashi Feng, and Hengshuang Zhao. Depth anything: Unleashing the power of large-scale unlabeled data. In *CVPR*, 2024. 2

[45] Lihe Yang, Bingyi Kang, Zilong Huang, Zhen Zhao, Xiaogang Xu, Jiashi Feng, and Hengshuang Zhao. Depth anything v2. In *NeurIPS*, 2024. 2, 3, 1

[46] Qiyi Yu, Quan Sun, Xiaosong Zhang, Yufeng Cui, Fan Zhang, Yue Cao, Xinlong Wang, and Jingjing Liu. Capsfusion: Rethinking image-text data at scale. In *CVPR*, 2024. 2

[47] Lu Yuan, Dongdong Chen, Yi-Ling Chen, Noel Codella, Xiyang Dai, Jianfeng Gao, Houdong Hu, Xuedong Huang, Boxin Li, Chunyuan Li, et al. Florence: A new foundation model for computer vision. *arXiv preprint arXiv:2111.11432*, 2021. 2

[48] Yuanwen Yue, Anurag Das, Francis Engelmann, Siyu Tang, and Jan Eric Lenssen. Improving 2d feature representations by 3d-aware fine-tuning. In *ECCV*, 2024. 6

[49] Xiaohua Zhai, Basil Mustafa, Alexander Kolesnikov, and Lucas Beyer. Sigmoid loss for language image pre-training. In *ICCV*, 2023. 1, 2, 3, 5, 8

[50] Bolei Zhou, Hang Zhao, Xavier Puig, Sanja Fidler, Adela Barriuso, and Antonio Torralba. Scene parsing through ade20k dataset. In *CVPR*, 2017. 6

[51] Jinghao Zhou, Chen Wei, Huiyu Wang, Wei Shen, Cihang Xie, Alan Yuille, and Tao Kong. ibot: Image bert pre-training with online tokenizer. In *ICLR*, 2022. 1, 2, 4

# Revisiting Multi-Task Visual Representation Learning

## Supplementary Material

### A. Additional Implementation Details

The main paper provides a high-level summary of our experimental setup while intentionally omitting certain lower-level details for clarity. In this section, we offer a more comprehensive account of the implementation and training configurations used in our experiments.

#### A.1. Data Curation

We adopt DataComp [12] as our pre-training source, which contains 1.1 billion image-text pairs. Due to download speed constraints, we were able to collect 200 million images from the full dataset. The downloading process spanned approximately 40 days and yielded nearly 21 TB of image-text pairs.

We use Depth Anything V2 (DA2-Large) [45] to generate a relative depth map for each image. The depth pipeline achieves a throughput of roughly 120K images per GPU-hour, requiring 13 hours to produce depth maps for 100M images on 64 GPUs. This high efficiency makes depth supervision straightforward to scale to larger corpora.

For grounding supervision, we sequentially apply RAM++ [17] to extract salient entity names and OWLv2-Base [29] to localize the referenced regions. This pipeline processes about 18K images per GPU-hour, resulting in 86 hours of processing time to generate region-text pairs for 100M images on 64 GPUs. Although slower than depth generation, the throughput remains sufficiently high to support billion-scale pseudo-label production.

#### A.2. Additional Training Details

**SSL Supervision.** The projection heads for self-distillation and masked prediction follow the same architecture but do not share parameters. Each head is a 3-layer MLP with L2 normalization, followed by a weight-normalized projection layer that maps to a 32k-dimensional prototype space.

The teacher network is updated as the exponential moving average (EMA) of the student using a fixed momentum of 0.994. To avoid representation collapse, we apply both centering and sharpening after the projection head. For *centering*, we maintain a running mean of student logits (momentum 0.9) and subtract this mean during training. For *sharpening*, we use a fixed student temperature of  $\tau_s = 0.1$  and linearly warm up the teacher temperature from  $\tau_t = 0.04$  to  $\tau_t = 0.07$ .

**Grounding Supervision.** As described in Section 4.3, we follow the CLOC approach [6] to utilize the grounding supervision. CLOC introduces a lightweight Transformer encoder, referred to as the **Prompter**, which extracts region-

specific visual features conditioned on bounding box locations. The **Prompter** takes three inputs: (i) the visual encoder output  $\mathbf{z}_i^*$  before final normalization and attentive pooling, (ii) a location embedding  $l_i$  derived from the bounding box coordinates (top-left and bottom-right), each encoded with positional embeddings, and (iii) a learnable query token  $\mathbf{o}$ . Given these inputs, the **Prompter** produces a regional visual feature  $\mathbf{o}_i = \text{Prompter}(\mathbf{z}_i^*, l_i, \mathbf{o})$ , which is then aligned to the regional text feature through the same contrastive formulation used in Equation 1.

**Depth Supervision.** The depth head follows the DPT [34] decoder, a convolutional module that fuses features from four intermediate layers of the visual encoder:  $\{3, 6, 9, 12\}$  for ViT-B/16 and  $\{6, 12, 18, 24\}$  for ViT-L/16.

As described in Section 4.3, we adopt the MiDaS objective [3], combining a scale- and shift-invariant loss with a multi-scale gradient matching loss.

Regarding the scale- and shift-invariant loss, the pseudo depth  $d$  and predicted depth  $\hat{d}$  are first normalized by:

$$d^* = \frac{d - t(d)}{s(d)}, \quad \hat{d}^* = \frac{\hat{d} - t(\hat{d})}{s(\hat{d})},$$

where  $t(d) = \text{median}(d)$ ,  $s(d) = \frac{1}{HW} \sum_{j=1}^{HW} |d - t(d)|$ . The scale- and shift-invariant (ssi) loss is then defined as:

$$\mathcal{L}_{\text{ssi}} = \frac{1}{2HW} \sum_{j=1}^{HW} |d_j^* - \hat{d}_j^*|.$$

To mitigate pseudo-label noise, we trim the 10% largest residuals. Let  $r_j = |d_j^* - \hat{d}_j^*|$  sorted in ascending order, we keep only the smallest  $U = 0.9HW$  residuals and define  $\mathcal{L}_{\text{ssitrim}} = \frac{1}{2HW} \sum_{j=1}^U r_j$ .

In addition, the gradient matching (gm) loss penalizes the depth discrepancies between the ground truth and the rescaled prediction across  $K = 4$  scales:

$$\mathcal{L}_{\text{gm}} = \sum_{k=1}^K \sum_{j=1}^{HW} \left( |\nabla_x^k d_j - s \nabla_x^k \hat{d}_j| + |\nabla_y^k d_j - s \nabla_y^k \hat{d}_j| \right),$$

where  $\nabla_x^k$  and  $\nabla_y^k$  denote finite differences along the horizontal and vertical directions at scale  $k$ .

The final depth loss is a weighted combination:

$$\mathcal{L}_{\text{depth}} = \mathcal{L}_{\text{ssitrim}} + 2 \times \mathcal{L}_{\text{gm}}.$$

**Computational Cost.** For the largest 100M-scale multi-task setting, our ViT-Base is trained on 32 GPUs for 5.7 days, while ViT-Large requires 64 GPUs for 9.4 days.

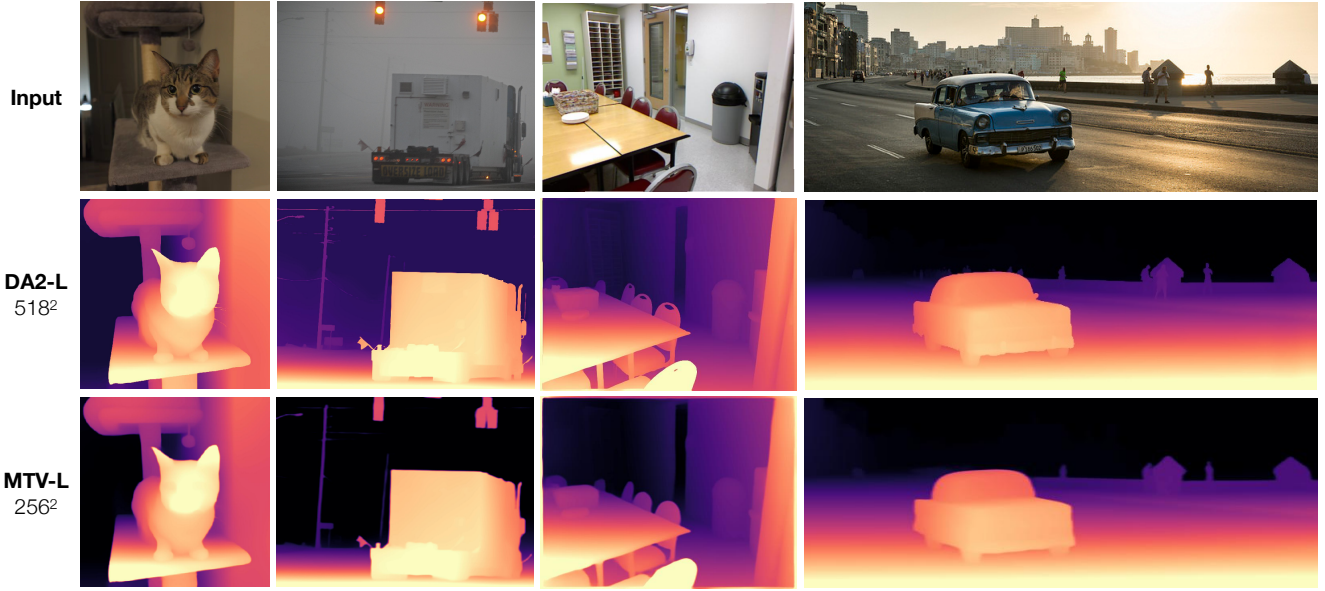


Figure 4. Visualizations of zero-shot relative depth estimation.

Table 6. **Zero-shot relative depth estimation.** We report the AbsRel metric (lower  $\downarrow$  is better).

Model	Input	KITTI $\downarrow$	NYUv2 $\downarrow$
Marigold [22]	480 $\times$ 640	9.9	5.5
DAv1-B [44]	518 $\times$ 518	8.0	4.6
DAv2-B [45]	518 $\times$ 518	7.8	4.9
MTV-B	224 $\times$ 224	8.9	6.0
MiDaS v3.1 [3]	518 $\times$ 518	12.7	4.8
DAv1-L [44]	518 $\times$ 518	7.6	4.3
DAv2-L [45]	518 $\times$ 518	7.4	4.5
MTV-L	256 $\times$ 256	8.2	5.2

## B. Zero-shot Relative Depth Estimation

Since our model is pretrained with depth supervision, we evaluate its zero-shot relative depth estimation performance against state-of-the-art depth models. We report AbsRel on KITTI [13] and NYUv2 [37], as shown in Table 6. Despite being trained in a multi-task setting and at substantially lower input resolution than specialized depth models (e.g., DA v1/v2 at 518<sup>2</sup>), our model achieves competitive zero-shot performance on both benchmarks.

Beyond quantitative results, Figure 4 further illustrates the qualitative comparisons. Our model produces depth maps with correct global geometry and coherent scene layout across diverse images. Compared with the depth-specialized DA2 model, certain fine details (e.g., the cat’s whiskers or the chair back) appear less sharp due to the resolution difference. Nevertheless, the predictions

remain stable and accurate overall, showing that low-resolution, pseudo-labeled depth supervision, when integrated into multi-task pretraining, can yield strong and well-generalized geometric representations.

## C. Limitations and Future Work

While our study provides a systematic examination of multi-task visual pretraining, several limitations remain.

**Scale of training data.** Our experiments are conducted on up to 100M image–text pairs with pseudo labels, which is substantially smaller than the 10B-scale corpora used by state-of-the-art VL models such as SigLIP2. Although our results demonstrate strong gains even under limited data, exploring whether multi-task supervision continues to scale at billion-level datasets remains an important direction.

**More dedicated data filtering.** Our pseudo labels are generated automatically without extensive filtering. As a result, some images exhibit low-quality captions, noisy grounding annotations, or unreliable depth estimates. While our analysis shows that these imperfections do not affect the overall conclusions, developing more refined data cleaning pipelines—or adaptive methods that handle noisy dense supervision—could further improve representation quality.

**Extending multi-task supervision beyond images.** Our current formulation focuses on single-view image pretraining. Incorporating additional modalities such as multi-view imagery or videos could unlock richer supervision signals. These extensions would allow integrating tasks like 3D reconstruction, motion flow, or video-language alignment, further pushing towards universal visual representations.